Location of the Iron−Sulfur Clusters F_A and F_B in Photosystem I: An Electron Paramagnetic Resonance Study of Spin Relaxation Enhancement of P_{700}^{+}†

K. V. Lakshmi,‡ Yean-Sung Jung,§,|| John H. Golbeck,*,⊥ and Gary W. Brudvig*,‡

Department of Chemistry, Yale University, New Haven, Connecticut 06520-8107, Department of Biochemistry and Molecular Biology, The Pennsylvania State University, University Park, Pennsylvania 16802-4500, and Department of Biochemistry, University of Nebraska, Lincoln, Nebraska 68502

Received May 11, 1999; Revised Manuscript Received July 20, 1999

ABSTRACT: Photosystem I (PS I) mediates electron-transfer from plastocyanin to ferredoxin via a photochemically active chlorophyll dimer (P_{700}), a monomeric chlorophyll electron acceptor (A_0), a phylloquinone (A_1), and three [4Fe-4S] clusters ($F_{X/A/B}$). The sequence of electron-transfer events between the iron−sulfur cluster, F_X, and ferredoxin is presently unclear. Owing to the presence of a 2-fold symmetry in the PsaC protein to which the iron−sulfur clusters F_A and F_B are bound, the spatial arrangement of these cofactors with respect to the C_2-axis of symmetry in PS I is uncertain as well. An unequivocal determination of the spatial arrangement of the iron−sulfur clusters F_A and F_B within the protein is necessary to unravel the complete electron-transport chain in PS I. In the present study, we generate EPR signals from charge-separated spin pairs (P_{700}^{+}-$F_{X/A/B}^{red}$) in PS I and characterize them by progressive microwave power saturation measurements to determine the arrangement of the iron−sulfur clusters $F_{X/A/B}$ relative to P_{700}. The microwave power at half saturation ($P_{1/2}$) of P_{700}^{+} is greater when both F_A and F_B are reduced in untreated PS I than when only F_A is reduced in mercury-treated PS I. The experimental $P_{1/2}$ values are compared to values calculated by using P_{700}-$F_{A/B}$ crystallographic distances and assuming that either F_A or F_B is closer to $P700^{+}$. On the basis of this comparison of experimental and theoretical values of spin relaxation enhancement effects on P_{700}^{+} in P_{700}^{+} $[4Fe\text{-}4S]^{-}$ charge-separated pairs, we find that iron−sulfur cluster F_A is in closer proximity to P_{700} than the F_B cluster.

Photosynthetic reactions involve a series of photoinduced charge separations coupled with rapid electron transfer in the reaction centers photosystems I and II (PS I and II, respectively). Photosystem II catalyzes water oxidation on the lumenal side of the thylakoid membrane while photosystem I is a chlorophyll-multisubunit protein complex that catalyzes the second photochemical reaction in electron-transfer from water to $NADP^{+}$. PS I is known to contain three [4Fe-4S] clusters ($F_{X/A/B}$) as well as other redox active cofactors including a photochemically active chlorophyll dimer (P_{700}), a monomeric chlorophyll electron acceptor (A_0), and a phylloquinone (A_1) that participate in electron transfer. Although the presence of electron transfer from the primary donor, P_{700}, to ferredoxin via the redox cofactors A_0, A_1 and F_X is well established, the precise sequence of electron-transfer events between the iron−sulfur cluster, F_X, and ferredoxin remains unclear (*1*).

A recently published 4.0 Å resolution X-ray crystallography structure by Krauss et al. (*2*, *3*) unambiguously assigns the location of the P_{700} chlorophylls, the accessory chlorophylls, the electron acceptor (A_0), and the iron−sulfur cluster F_X in PS I. Although it is possible to determine the separation between the terminal iron−sulfur electron-acceptors F_A and F_B (12 Å) at this resolution, the two centers are indistinguishable in this structure due to a pseudo 2-fold symmetry in the PsaC protein to which they are bound. The electron density map shows that the F_A-F_B vector is 52° with respect to membrane plane suggesting sequential electron transfer from F_A to F_B (*2*, *3*). There have been a number of studies conducted to probe indirectly the sequence of electron transfer between F_X and ferredoxin. Kinetics of electron transfer in Hg-treated PS I suggest that F_B is an intermediate donor to ferredoxin and flavodoxin (*4*, *5*) and electrogenicity studies on the acceptor side suggest that F_A (rather than F_B) is proximal to F_X (*6*), indicating that F_B may be the electron donor to ferredoxin. The EPR properties of in vitro and in vivo mutants of the cysteine ligands to the [4Fe-4S] clusters provide a biochemical argument that PsaC is oriented so that F_A is proximal to, and F_B is distal to, F_X (*7*). Studies involving selective destruction of F_B by either the use of urea-ferricyanide (*8*) or Hg-treatment (*9*−*13*) also imply that F_B is closer to the protein surface, increasing the possibility of attack by such reagents. Contrary to this picture, mutagenesis studies show that the D9A mutant does not bind F_X, which might be an indication that there is a preferential

† This work was supported by Grant GM36442 from the National Institutes of Health (G.W.B.) and Grant MCB-9723661 from the National Science Foundation (J.H.G.).

* To whom correspondence should be addressed. (J.H.G.) Phone: (814) 865-1163. Fax: (814) 863-7024. E-mail: JHG5@psu.edu. (G.W.B.) Phone: (203) 432-5202. Fax: (203) 432-6144. E-mail: gary.brudvig@yale.edu.

‡ Department of Chemistry, Yale University.

§ Department of Biochemistry, University of Nebraska.

|| Present address: Department of Biochemistry, University of California, Irvine.

⊥ Department of Biochemistry and Molecular Biology, The Pennsylvania State University.

10.1021/bi9910777 CCC: $18.00
Published on Web 09/03/1999

arrangement in the reaction center where F_B is closer to F_X than to the ferredoxin (*14*). Historically, the midpoint potentials of the three iron−sulfur clusters and increased photoreduction of F_A over F_B at cryogenic temperature have been invoked to suggest electron-transfer events that involve a linear sequence of transfer from F_X to F_A via F_B where F_A is the terminal acceptor in the electron-transfer chain (*15*) (reviewed in ref *1*).

To date, there remains a lingering uncertainty regarding the identity of the terminal acceptor in the electron transport chain to ferredoxin as well as the kinetic rates of the discrete electron-transfer steps involved. Also, the issue of whether both clusters are really essential for electron-transport to ferredoxin is presently unresolved, i.e., is the flow of electrons serial through F_A and F_B (as implied by midpoint potentials) or is it parallel from F_X to either F_A or F_B. An unambiguous determination of the spatial arrangement of the iron−sulfur clusters F_A and F_B within the protein is key to understanding the chain of terminal electron-transport events in PS I. Spin relaxation behavior of an EPR-active species provides information on magnetic environments and interspin distances between spatially connected paramagnetic species. In the present study, we generate EPR signals from charge-separated spin pairs (P_{700}^+-$F_{X/A/B}^-$) in PS I and characterize them via microwave power saturation measurements to determine the arrangement of the iron−sulfur clusters $F_{X/A/B}^-$ relative to P_{700}^+. The experimental data are compared to values calculated by using P_{700}−$F_{A/B}$ crystallographic distances and assuming that either F_A or F_B is closer to $P700^+$. These results show that F_A is proximal to P_{700}.

MATERIALS AND METHODS

Preparation of Charge-Separated P_{700}^+-[4Fe-4S]$^-$ Pairs in PS I. Wild-type PS I complexes were isolated from *Synechococcus* sp. by previously published procedures (*16*). Mercury-treated F_B-depleted PS I was prepared by the procedure of Jung et al. (*13*), which is a modification of published techniques (*9*) suited for cyanobacteria. F_A/F_B-depleted PS I was prepared by the method of Parrett et al. (*17*). Unless otherwise mentioned, the samples were resuspended in a buffer containing 50 mM Tris(hydroxymethyl)-aminomethane (Tris), 0.05% Triton X-100, and 20% glycerol at pH 7.0. $P_{700}^+F_A^{ox}F_B^{ox}F_X^{ox}$ was chemically induced in wild-type PS I by oxidation with minimal concentrations (<0.05 mM) of potassium ferricyanide [$K_3Fe(CN)_6$] at pH 7.0. $P_{700}^+F_A^{red}$ was photoinduced in wild-type PS I and Hg-treated, F_B-depleted PS I by illumination at 77 K following the addition of 1 mM sodium ascorbate and 1 mM tetramethyl-*p*-phenylenediamine (TMPD) at pH 7.0. $P_{700}^+F_A^{red}F_B^{red}$ was photoinduced by illumination at 77 K in wild-type PS I in a buffer containing 0.1 M glycine, 0.05% Triton X-100, 50 mM dithionite, and 20% glycerol at pH 10.0. Here, dithionite reduction produced P_{700} $F_X^{ox}F_A^{red}F_B^{red}$ (∼90%) and P_{700} $F_X^{ox}F_A^{red}F_B^{ox}$ (∼10%), which upon photoreduction yields $P_{700}^+F_X^{red}F_A^{red}F_B^{red}$ and $P_{700}^+F_X^{ox}F_A^{red}F_B^{red}$, respectively. However, $P_{700}^+F_X^{red}$ charge-separated pairs decay in the dark resulting in a mixture of $P_{700}^+F_X^{ox}F_A^{red}F_B^{red}$ and P_{700} $F_X^{ox}F_A^{red}F_B^{red}$ so that the P_{700}^+ species observed in the EPR experiment is magnetically coupled to the $F_A^{red}F_B^{red}$ pair. $P_{700}^+F_X^{red}$ was photoinduced by illumination at 20.0 K in F_A/F_B-depleted PS I at pH 7.0 following the addition of 1 mM sodium ascorbate and 1 mM TMPD. EPR data acquisition for the P_{700}^+-$F_A^{red}/F_B^{red}/F_A^{red}F_B^{red}$ samples was conducted in the dark to avoid interference from P_{700}^+-F_X^{red} pairs. P_{700}^+-F_X^{red} measurements in F_A/F_B-depleted PS I were conducted under continuous illumination due to the short lifetime of this charge-separated state in the absence of light. Chlorophyll concentrations in all the samples were typically ∼1.0 mg/mL except for the F_B-depleted mercury-treated PS I sample (0.4 mg/mL).

EPR Spectroscopy. All EPR measurements were performed on a Varian E−9 spectrometer (operating at a frequency of 9.28 GHz) equipped with a TE_{102} cavity and a helium flow cryostat (Oxford Instruments). PS I samples were loaded into 4 mm quartz tubes (Wilmad Glass) and the samples were repeatedly degassed prior to EPR measurements to ensure the absence of relaxation enhancement due to triplet oxygen (*18*) (unless otherwise mentioned). All power saturation measurements were carried out at 20 K. Typically 4−6 spectra were acquired per data point in the microwave power saturation curves and the intensities were measured from the peak-to-trough heights of the P_{700}^+ EPR signals.

Spin−Lattice Relaxation Enhancement Measurements. Long-range interactions (r > 10 Å) between a pair of electron spins (i and j) are mainly comprised of dipolar couplings. The field experienced by the species i is a combination of the applied magnetic field, B_0, and a local fluctuation caused by spin flips of the species j. If the species j has a rapid spin−lattice relaxation rate, T_{1j}, the local field fluctuations enhance the spin−lattice relaxation rate of the species i as given in eq 1,

$$1/T_{1i,\text{observed}} = 1/T_{1i,\text{intrinsic}} + 1/T_{1i,\text{dipolar}} \quad (1)$$

where, $T_{1i,\text{observed}}$ is the measured spin−lattice relaxation rate of the i spins in the presence of the fast-relaxing j spins and $T_{1i,\text{intrinsic}}$ and $T_{1i,\text{dipolar}}$ are the intrinsic and dipolar-enhanced relaxation rates of the i spins. The spin−lattice relaxation enhancement observed for the species i due to a dipolar interaction with the fast-relaxing species j will display an r^{-6} distance dependence.

Progressive microwave power saturation is a well-established technique to estimate spin−lattice relaxation enhancement of a slow-relaxing species in the presence of a fast-relaxing species (*19*, *20*). The half-power at which an EPR-active species saturates ($P_{1/2}$) is a direct reflection of its spin−lattice relaxation rate (T_1) as given in eq 2,

$$P_{1/2i} \propto 1/(\gamma^2 T_{1i} T_{2i}) \quad (2)$$

where γ is the electron magnetogyric ratio. The EPR signal amplitude (A) is related to the observe microwave power (P) by eqs 3 and 4 (*21*):

$$A = K\sqrt{P}/(1 + P/P_{1/2i})^{b/2} \quad (3)$$

$$\log(A/\sqrt{P}) = -b/2 \log(P_{1/2i} + P) + \text{constant} \quad (4)$$

Thus, a least-squares curve fit of $\log(A/\sqrt{P})$ as a function of $\log P$ would yield an estimate of the half-power at which the species i saturates ($P_{1/2i}$). Furthermore, because

$$P_{1/2i,\text{observed}} = P_{1/2i,\text{intrinsic}} + P_{1/2i,\text{dipolar}} \quad (5)$$

the $P_{1/2i,\text{dipolar}}$ values can estimated experimentally by measuring the power saturation of the slow-relaxing species *i* in the presence ($P_{1/2i,\text{observed}}$) and absence ($P_{1/2i,\text{intrinsic}}$) of the fast-relaxing species *j*. A direct comparison of the relative magnitudes of $P_{1/2i}$ of the slow-relaxing species (P_{700}^+) in the presence of different fast-relaxers ($F_{X/A/B}^{red}$) yields a qualitative estimate of the interspin distance between the various charge-separated pairs in PS I using eq 6:

$$P_{1/2i,\text{dipolar}} = \text{constant}/r^6 \quad (6)$$

RESULTS AND DISCUSSION

In the present study, we utilize the technique of progressive power saturation to measure the spin relaxation enhancement of P_{700}^+ centers due to dipolar interactions with reduced iron−sulfur clusters in charge-separated P_{700}^+ $[4Fe\text{-}4S]^-$ pairs in PS I. On the basis of the recent X-ray crystallography structure published by Fromme and co-workers (*2*), the special pair of chlorophyll moieties constituting the primary donor (P_{700}) in PS I is fairly exposed to the external surface of the protein making them readily accessible to the bulk solvent (and dissolved paramagnetic molecules). Thus, in addition to spin−lattice relaxation-enhancement of the P_{700}^+ radicals due to dipolar interactions with reduced iron−sulfur clusters within the charge-separated pairs in PS I, P_{700}^+ radicals may also exhibit additional relaxation enhancement due to the presence of chemical oxidants or triplet oxygen in these samples (*18*). To determine the magnitude of these effects, we compare progressive power saturation curves of P_{700}^+ radicals (both chemically induced and photoinduced) under aerobic and anaerobic conditions. Shown in Figure 1 is a comparison of the power saturation behavior of photoinduced P_{700}^+ in the charge-separated pair $P_{700}^+F_A^{red}F_B^{ox}F_X^{ox}$ (in wild-type ascorbate-treated PS I) (Figure 1a) and chemically induced P_{700}^+ (in the presence of 1, 2, and 10 mM ferricyanide) (Figure 1, panels b−d) under aerobic and anaerobic sample conditions. As can be seen in this figure, the spin relaxation rates of the P_{700}^+ radical in the anaerobic samples are lower than those observed in the aerobic samples. This indicates that the P_{700}^+ radicals experience significant spin relaxation enhancement due to dipolar and exchange interactions with paramagnetic triplet oxygen present in the aerobic PS I samples. Thus, to isolate the relaxation effects expected from the presence of the reduced iron−sulfur clusters in the various charge-separated pairs, it is critical that the progressive power saturation measurements be conducted under anaerobic conditions.

To facilitate comparison between the P_{700}^+ relaxation enhancement due to the presence of the iron−sulfur clusters F_A, F_B, and F_X in PS I, it is important to determine the intrinsic relaxation rate of a noninteracting P_{700}^+ radical in the native protein environment. This can be achieved by chemically generating a P_{700}^+ radical by the addition of an external oxidant (ferricyanide). However, the presence of excess paramagnetic ferricyanide ions in the system could potentially enhance the spin−lattice relaxation rates of P_{700}^+ and interfere with the observation of relaxation effects solely due to the presence of fast-relaxing reduced iron−sulfur clusters. Shown in Figure 1e is a plot of the $P_{1/2}$ values of chemically induced P_{700}^+ in wild-type PS I samples as a function of the ferricyanide concentration used. A best linear fit for the data points indicates that, at concentrations of 0.05 mM ferricyanide or less, contributions to relaxation enhancement of P_{700}^+ from ferricyanide ions are negligible.

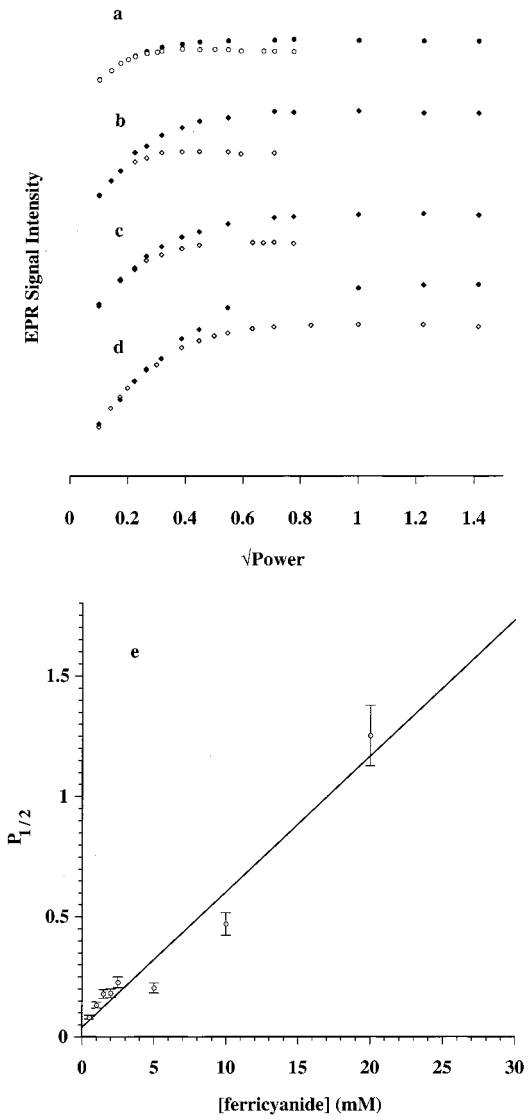

FIGURE 1: Progressive microwave power saturation measurements of P_{700}^+ in aerobic (closed symbols) and anaerobic (open symbols) PS I samples: (a) photoinduced P_{700}^+ in the charge-separated pair $P_{700}^+F_A^{red}F_B^{ox}F_X^{ox}$ (in wild-type ascorbate-treated PS I) and chemically generated P_{700}^+ in wild-type PS I containing (b) 1 mM, (c) 2 mM or (d) 10 mM ferricyanide, and (e) the dependence of $P_{1/2}$ values of chemically induced P_{700}^+ in PS I on the ferricyanide concentration in the medium. The data in parts a−d have been offset vertically for clarity. Indicated on the data points in part e are 10% error bars that account for small variations observed in the least-squares fits that yield experimental $P_{1/2}$ values as well as errors in technique. The solid line in part e is the best weighted linear fit obtained for the ferricyanide concentration dependence of P_{700}^+ $P_{1/2}$ values. All the $P_{1/2}$ values shown in part e were obtained under anaerobic sample conditions.

In a progressive power saturation measurement, the half-power at which an EPR-active species saturates ($P_{1/2}$) is a direct reflection of its spin−lattice relaxation rate. We expect enhancement of the intrinsic spin−lattice relaxation rate of a slow-relaxing P_{700}^+ radical in the presence of a fast-relaxing $[4Fe\text{-}4S]^-$ cluster in isolated charge-separated pairs in the PS I reaction centers. The magnitude of the enhancement observed depends on the interspin distance (*r*). A measure of $P_{1/2}$ values for P_{700}^+ in the various charge-separated pairs

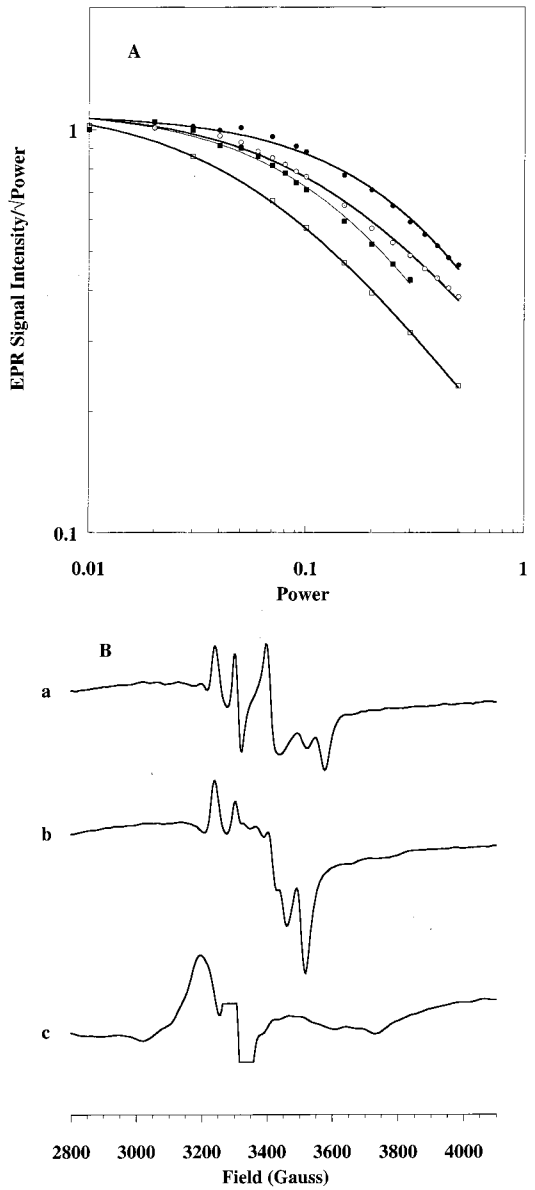

FIGURE 2: (A) Progressive power saturation measurements of chemically generated P_{700}^+ (□) and P_{700}^+ in the charge-separated pairs $P_{700}^+F_A^{red}$ (■), $P_{700}^+F_A^{red}F_B^{red}$ (○), and $P_{700}^+F_X^{red}$ (●). Solid lines indicate the least-squares curve fits of $\log(A/\sqrt{P})$ as a function of $\log P$ (eq 4) and yield an estimate of the $P_{1/2}$ values of P_{700}^+ in the absence and presence of the iron−sulfur clusters. (B) EPR spectra of the iron−sulfur clusters in the photoinduced charge-separated pairs: (a) $P_{700}^+F_A^{red}$ in wild-type ascorbate-treated PS I, (b) $P_{700}^+F_A^{red}F_B^{red}$ in wild-type dithionite-treated PS I, (c) $P_{700}^+F_X^{red}$ in F_A/F_B-depleted PS I at pH 7.0. The central region of the spectrum in part c has been deleted due to interference from the P_{700}^+ EPR signal. Experimental parameters: microwave frequency = 9.28 GHz; magnetic field modulation frequency = 100 kHz; modulation amplitude = 20 G; microwave power = 20.0 mW for parts a and b and 40 mW for part c, respectively; temperature = 7.8, 20.0, and 6.0 K for parts a, b and c, respectively.

will yield a qualitative estimate of distances (*21*) between the chlorophyll primary donor and [4Fe-4S] clusters. Shown in Figure 2A is a logarithmic plot of the ratio of P_{700}^+ EPR signal intensities to the square-root of observe microwave power as a function of the observe microwave power used. The $P_{1/2}$ values were determined by least-squares computer fits to the experimental data (eq 4) (*21*). As can be seen in Figure 2A, the intrinsic spin relaxation rate of a noninteracting chemically generated P_{700}^+ radical is slower than that in the charge-separated pairs $P_{700}^+F_A^{red}$ (in Hg-treated F_B-depleted PS I), $P_{700}^+F_A^{red}F_B^{red}$ (in dithionite-treated PS I), and $P_{700}^+F_X^{red}$ (in F_A/F_B-depleted PS I). The $P_{1/2}$ values shown in Table 1 indicate that P_{700}^+ does indeed exhibit enhanced relaxation rates in the presence of the fast-relaxing iron−sulfur clusters F_A, F_B, and F_X. Comparison of individual progressive power saturation curves for P_{700}^+ in the charge-separated $P_{700}^+F_A^{red}$, $P_{700}^+F_A^{red}F_B^{red}$, and $P_{700}^+F_X^{red}$ pairs indicates a maximum spin relaxation enhancement in $P_{700}^+F_X^{red}$ consistent with crystallographic data showing that F_X is in much closer proximity to P_{700}. Observation of the $P_{700}^+F_X^{red}$ pair in F_A/F_B-depleted PS I isolates the relaxation enhancement solely due to the presence of F_X^{red}. A different approach was used in previous relaxation measurements (*22*) where the enhancement due to F_X^{red} was determined in the presence of all three iron−sulfur clusters, F_A^{red}, F_B^{red}, and F_X^{red}, and it was assumed that the relaxation enhancement due to F_A^{red} and F_B^{red} is negligible in comparison to F_X^{red}. Thus, the spin−lattice relaxation rate enhancement and P_{700}−F_X distance determined previously in the presence of F_A^{red} and F_B^{red} are approximate values. A comparison between the power saturation data for $P_{700}^+F_A^{red}$ and $P_{700}^+F_A^{red}F_B^{red}$ shows that P_{700}^+ relaxation rates in the presence of F_A^{red} alone and $F_A^{red}F_B^{red}$ together are comparable. Given that the spin−lattice relaxation rates of the F_A^{red} and F_B^{red} iron−sulfur clusters are comparable (*22*) and the two clusters display similar microwave power saturation behavior (J. H. Golbeck, unpublished results), this is direct evidence for F_A being closer to P_{700} than F_B.

Table 1: Experimental and Calculated $P_{1/2}$ Values of P_{700}^+

species	$P_{1/2}$, exptl (mW)	$P_{1/2}$, calcd[a] (mW)	$P_{1/2}$, calcd[b] (mW)
P_{700}^+ (ferricyanide-treated PS I)	0.080		
$P_{700}^+F_A^{red}$ (Hg-treated F_B-depleted PS I)	0.122		
$P_{700}^+F_A^{red}F_B^{red}$ (wt dithionite-treated PS I)	0.145	0.140	0.478
$P_{700}^+F_X^{red}$ ($F_{A/B}$-depleted PS I)	0.213		

[a] Assuming that the iron-sulfur cluster F_A is proximal to P_{700}. [b] Assuming that the iron-sulfur cluster F_A is distal to P_{700}.

Shown in Figure 2B are EPR signals of the iron−sulfur clusters in each of the charge-separated states that identify the individual [4Fe-4S] species present, namely, $P_{700}^+F_A^{red}$, $P_{700}^+F_A^{red}F_B^{red}$, and $P_{700}^+F_X^{red}$. Upon comparison with previously published experimental and simulated EPR spectra of iron−sulfur clusters in PS I (*1*), it can be seen that the samples used in the present study contain high photoinduced yields of the individual charge-separated pairs $P_{700}^+F_A^{red}$ (in wild-type ascorbate-treated PS I), $P_{700}^+F_A^{red}F_B^{red}$ (in wild-type dithionite-treated PS I), and $P_{700}^+F_X^{red}$ (in $F_{A/B}$-depleted PS I). The EPR spectra of $P_{700}^+F_A^{red}$ and $P_{700}^+F_A^{red}F_B^{red}$ in Figure 2B exhibit *g*-values of 1.86, 1.94, and 2.05 and 1.89, 1.92, 1.94, and 2.05, which are typical of noninteracting F_A^{red} and interacting F_A^{red} and F_B^{red} iron−sulfur clusters, respectively. Furthermore, the absence of a peak at $g = 1.86$ in part b indicates that there is no contribution from $P_{700}^+F_A^{red}F_B^{ox}$

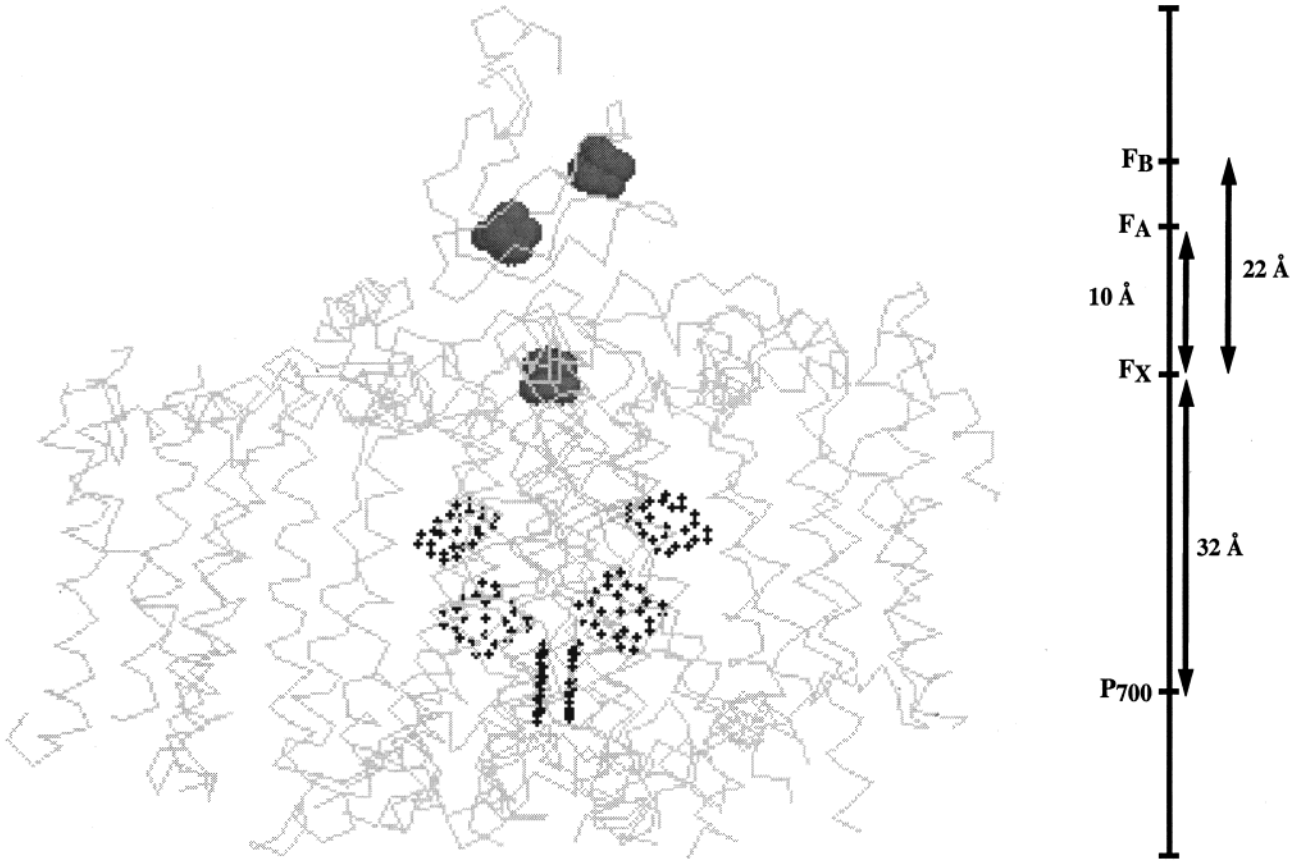

FIGURE 3: A combined model based on the X-ray coordinates[1] (3) of PS I and the arrangement of cofactors based on EPR spin relaxation enhancement studies. The P_{700} F_X, P_{700} F_A and P_{700} F_B distances are from the X-ray coordinates and the spatial assignment of F_A and F_B is based on the $P_{1/2}$ values calculated in the present study.

charge-separated pairs in the dithionite-treated photoreduced PS I samples.

Shown in Table 1 are the experimental $P_{1/2}$ values for P_{700}^+ radicals in the presence of F_A^{red}, $F_A^{red}F_B^{red}$, and F_X^{red}. Also shown are calculated $P_{1/2}$ values of P_{700}^+ radicals interacting with $F_A^{red}F_B^{red}$ (in dithionite-treated PS I). The P_{700}^+ $P_{1/2}$ value for $P_{700}^+F_A^{red}$ is used as a calibration point in this table for the calculated $P_{1/2}$ value of $P_{700}^+F_A^{red}F_B^{red}$. Using the evidence that the spin−lattice relaxation rates of the F_A^{red} and F_B^{red} iron−sulfur clusters are comparable (22), the r^{-6} dependence of the spin-relaxation enhancement (eq 6) and the relative $P_{700}-F_{A/B}$ distances (42 and 54 Å, respectively) from the X-ray crystallography data (*2*), we estimate the expected magnitude of spin−lattice relaxation enhancement effects on the $P_{1/2}$ values of P_{700}^+ in the $P_{700}^+F_A^{red}F_B^{red}$ charge-separated state. As can be seen in Table 1, the predicted value of $P_{1/2}$ of P_{700}^+ in the $P_{700}^+F_A^{red}F_B^{red}$ state is in good agreement with the experimentally determined value when it is assumed that F_A is closer to P_{700}. The calculation using the reverse assumption that the $P_{700}-F_A$ and $P_{700}-F_B$ distances are 54 and 42 Å, respectively, yields a value that is not in agreement with the experimentally observed $P_{1/2}$ value obtained in this study.

Single-crystal EPR data on the iron−sulfur clusters, F_A and F_B, in conjunction with structural data on bacterial 2[4Fe-4S] ferredoxins and electron density maps from Fromme and co-workers (*2*, *3*) have been used to model the orientation of the PsaC protein that contains F_A and F_B (*23*, *24*). Unfortunately, the local pseudo C_2-symmetry axis inherent to the ferredoxin model leaves a 2-fold ambiguity in their conclusions. Kamlowski et al. (*23*) conclude that either F_A or F_B could be the proximal to F_X. Previous spin−lattice relaxation and transient EPR measurements on PS I have focused on the distances between $P_{700}-F_X$, A_1-F_X, A_0-F_X (*22*, *25*, *26*), and $P_{700}-A_1$ (*27*). The distances determined in these studies mainly address the spatial location of the P_{700}, A_1, A_0 cofactors relative to the F_X iron−sulfur cluster in PS I. In the present study, we unambiguously determine the relative spatial orientation of the three iron−sulfur clusters in PS I. On the basis of progressive microwave power saturation data, we conclude that F_A is the cluster that is proximal to F_X and F_B is the terminal cluster.

Figure 3 shows a schematic of the 4.0 Å X-ray coordinates[1] determined by Fromme and co-workers (*2*, *3*). As can be seen in this structure, F_X is at a distance of 32 Å from the chlorophyll special pair, P_{700}. Combining the "EPR ruler" obtained from the progressive microwave power saturation data in the present study with the X-ray crystallography structure, we conclude that F_A is in closer proximity to F_X and is at a distance of 42 Å from P_{700} and F_B is placed such that it is the terminal iron−sulfur cluster in PS I (54 Å from P_{700}). Saturation-recovery EPR measurements are currently in progress to measure precise spin−lattice relaxation rates

[1] Coordinates for the theoretical model of the photosystem I reaction center were taken from the protein data bank (*28*, *29*) (entry, 2PPS; N. Krauss, W.-D. Schubert, O. Klukas, P. Fromme, H. T. Witt, W. Saenger, 1996) (*2*) and were visualized using the software program "Swiss-PDB viewer" (Glaxo Wellcome Experimental Research, Geneva, Switzerland).

of P_{700}^+ in the charge-separated pairs and thus determine precise distances between the special pair of chlorophylls and F_X/F_A using EPR spectroscopy.

REFERENCES

1. Golbeck, J. H., and Bryant, D. A. (1991) *Curr. Top. Bioenerget. 16*, 83−177.
2. Krauss, N., Schubert, W.-D., Klukas, O., Fromme, P., Witt, H. T., and Saenger, W. (1996) *Nat. Struct. Biol. 3*, 965−969.
3. Fromme, P., Witt, H. T., Schubert, W.-D., Klukas, O., Saenger, W., and Krauss, N. (1996) *Biochim. Biophys. Acta 1275*, 76−83.
4. Díaz-Quintana, A., Leibl, W., Bottin, H., and Sétif, P. (1998) *Biochemistry 37*, 3429−3439.
5. Vassiliev, I. R., Jung, Y. S., Yang, F., and Golbeck, J. H. (1998) *Biophys. J. 74*, 2029−2035.
6. Mamedov, M. D., Gourovskaya, K. N., Vassiliev, I. R., Golbeck, J. H., and Sememov, A. Y. (1998) *FEBS Lett. 431*, 219−223.
7. Golbeck, J. H. (1999) *Photosynth. Res. 61*, 107−144.
8. Golbeck, J. H., and Warden, J. T. (1982) *Biochim. Biophys. Acta 681*, 77−84.
9. Kojima, Y., Niinomi, Y., Tsuboi, S., Hiyama, T., and Sakurai, H. (1987) *Bot. Magn., Tokyo 100*, 243−253.
10. Fujii, T., Yokayama, E., Inoue, K., and Sakurai, H. (1990) *Biochim. Biophys. Acta 1015*, 41−48.
11. Sakurai, H., Inoue, K., Fujii, T., and Mathis, P. (1991) *Photosyn. Res. 27*, 65−71.
12. He, W., and Malkin, R. (1994) *Photosyn. Res. 41*, 381−388.
13. Jung, Y. S., Yu, L., and Golbeck, J. H. (1995) *Photosynth. Res. 46*, 249−255.
14. Rodday, S. M., Do, L. T., Chynwat, V., Frank, H. A., and Biggins, J. (1996) *Biochemistry 35*, 11832−11838.
15. Evans, M. C. W., Reeves, S. G., and Cammack, R. (1974) *FEBS Lett. 49*, 111−114.
16. Mehari, T., Parrett, K. G., Warren, P. V., and Golbeck, J. H. (1991) *Biochim. Biophys. Acta 1056*, 139−148.
17. Parrett, K. G., Mehari, T., Warren, P. V., and Golbeck, J. H. (1989) *Biochim. Biophys. Acta 973*, 324−332.
18. Galli, C., MacArthur, R. L., Abu-Soud, H. M., Clark, P., Steuhr, D. J., and Brudvig, G. W. (1996) *Biochemistry 35*, 2804−2810.
19. Portis, M. (1953) *Phys. Rev. 91*, 1071−1079.
20. Castner, T. G. (1959) *Phys. Rev. 115*, 1506−1515.
21. Galli, C., Innes, J. B., Hirsh, D. J., and Brudvig, G. W. (1996) *J. Magn. Reson., Ser. B 110*, 284−287.
22. Berry, M. C., Bratt, P. J., and Evans, M. C. W. (1997) *Biochim. Biophys. Acta 1319*, 163−176.
23. Kamlowski, A., van der Est, A., Fromme, P., Krauss, N., Schubert, W.-D., Klukas, O., and Stehlik, D. (1997) *Biochim. Biophys. Acta 1319*, 199−213.
24. Kamlowski, A., van der Est, A., Fromme, P., and Stehlik, D. (1997) *Biochim. Biophys. Acta 1319*, 185−198.
25. Deligiannakis, Y., Hanley, J., and Rutherford, A. W. (1998) *Biochemistry 37*, 3329−3336.
26. Bittl, R., Zech, S. G., Fromme, P., Witt, H. T., and Lubitz, W. (1997) *Biochemistry 36*, 12001−12004.
27. Bittl, R., and Zech, S. G. (1997) *J. Phys. Chem. B 101*, 1429−1436.
28. Sussman, J. L., Lin, D., Jiang, J., Manning, N. O., Prilusky, J., Ritter, O., and Abola, E. E. (1998) *Acta Crystallogr., Sect. D 54*, 1078−1084.
29. Abola, E. E., Sussman, J. L., Prilusky, J., and Manning, N. O. (1997) in *Protein Data Bank Archives of Three-Dimensional Macromolecular Structures*, *Methods in Enzymology* (Carter, C. W. J., and Sweet, R. M., Ed.) pp 556−571, Academic Press, San Diego.

BI9910777